

# Effect of Co/Mg ratio on the phase, microstructure, dielectric and impedance properties of lead zirconate titanate

A. Mahmood<sup>1,2</sup> · A. Naeem<sup>2</sup> · M. Y. Kaya<sup>1</sup> · M. Yasin<sup>3</sup> · E. Mensur-Alkoy<sup>4</sup> · S. Alkoy<sup>1</sup>

Received: 7 June 2015 / Accepted: 25 August 2015 / Published online: 3 September 2015  
© Springer Science+Business Media New York 2015

**Abstract** Polycrystalline  $\text{PbTi}_{0.5}\text{Zr}_{0.3}(\text{Co}_{1-x}\text{Mg}_x)_{0.2}\text{O}_3$  ( $x = 0.00, 0.25, 0.45, 0.65, 0.85$ ) ceramics were synthesized using sol–gel route at 1150 °C for 2 h in air. The final ceramics were characterized by X-ray diffraction (XRD), scanning electron microscopy and impedance spectroscopy. XRD studies confirmed the tetragonal symmetry ( $P4mm$ ) of the sintered ceramics. The dielectric constant ( $\epsilon_r$ ) was found to increase with increasing temperature in the given temperature regime (30–300 °C). Sample with  $x = 0.25$  exhibited high magnitude of  $\epsilon_r$  (4261) and dielectric loss ( $\tan\delta = 0.05$ ) over a wide range of temperature at 100 kHz. Magnitude of  $\tan\delta$  of the sample with  $x = 0.65$  was recorded to be 0.009 around room temperature at 100 kHz. Resistance of ceramic samples was decreased with an increase in temperature demonstrating a non-Debye type of relaxation process. The AC conductivity of  $\text{PbTi}_{0.5}\text{Zr}_{0.3}(\text{Co}_{1-x}\text{Mg}_x)_{0.2}\text{O}_3$  samples increased gradually with increasing temperature and frequency.

## 1 Introduction

Due to ever increasing demand on electronic devices, lead zirconate titanate ( $\text{PbZrTiO}_3$  or PZT) based ceramics are potential candidate materials for microelectronic applications, such as integrated circuits, transducers and actuators, because of their good piezoelectric and ferroelectric properties. For practical device applications thermally stable materials are required due to abrupt changes in the dielectric response around transition temperature [1, 2]. The dielectric properties of PZT can be tailored by using various isovalent and aliovalent dopants on either A-site ( $\text{Rb}^+$ ,  $\text{K}^+$ ,  $\text{Na}^+$ ) or B-site ( $\text{Fe}^{2+}$ ,  $\text{Fe}^{3+}$ ,  $\text{Mg}^{2+}$ ,  $\text{Sc}^{3+}$ ,  $\text{Co}^{3+}$ ). Various attempts have been reported to improve the electrical properties of PZT [3, 4]. Rai et al. [5] reported diffused phase transition (DPT) for the Fe and Mn co-doped lead lanthanum zirconate titanate (PLTZ) ceramics in the temperature regime (300–600 K) at 10 kHz. The phase transition temperature ( $T_c$ ) was observed to shift toward high temperature with a decrease in the Zr content. Randall et al. [6] reported that domain wall contribution in the donor-doped PZT was strongly influenced by grain size. Furthermore, an increase in the  $\tan\delta$  that was observed with a decrease in the grain size was attributed to an increase in the domain density. Jiang et al. [7] investigated the effect of Zr/Sn ratio in the lead lanthanum zirconate stannate titanate ( $\text{Pb}_{0.87}\text{Ba}_{0.1}\text{La}_{0.02}(\text{Zr}_x\text{Sn}_{0.95-x}\text{Ti}_{0.05})\text{O}_3$  (PBLZST;  $x = 0.6–0.8$ ) ceramic systems. A high saturation polarization ( $43.5 \mu\text{C}/\text{cm}^2$ ) was reported for the sample with  $x = 0.675$ . The Zr/Sn ratio was reported to be effective for tuning the electrical properties of PBLZST ceramics.

Doped PZT can be prepared by a variety of methods, such as conventional solid state sintering route, peroxo-hydroxide method, citrate precursor method, precipitation method, hydrothermal method and sol–gel method. Solid

✉ S. Alkoy  
sedal@gtu.edu.tr

<sup>1</sup> Department of Materials Science and Engineering, Gebze Technical University, 41400 Gebze, Kocaeli, Turkey

<sup>2</sup> National Centre of Excellence in Physical Chemistry, University of Peshawar, Peshawar 25120, Pakistan

<sup>3</sup> National University of Sciences and Technology, 44000 Islamabad, Pakistan

<sup>4</sup> Faculty of Engineering and Natural Sciences, Maltepe University, Istanbul, Turkey

state sintering route suffers from the contaminations due to the involvement of various steps and subsequent heat treatment at high temperature. Sol–gel method offers various advantages over other synthesis procedures, such as modified doping mechanism, high purity of product, ease of preparation, good dispersion and control over stoichiometry in the complex solid solution systems [8–10]. In sol–gel method, macromolecule network of metallic oxide is formed by hydrolysis and subsequent condensation reactions, and the coordination of central metallic ion can be adjusted by various chemical reagents.

In the present study polycrystalline  $\text{PbTi}_{0.5}\text{Zr}_{0.3}(\text{Co}_{1-x}\text{Mg}_x)_{0.2}\text{O}_3$  ceramics were synthesized by sol–gel method. The effect of Co/Mg ratio on the phase, microstructure and dielectric properties were investigated in detail. A limited amount of literature is available on the Co or Mg doped PZT ceramics but effect of Co and Mg co-doped PZT ceramics have not been reported previously to the best of our knowledge. Mg doped PZT ceramics exhibit activation energy ( $E_a \approx 1.05$  eV) which is comparable with the  $E_a$  values (1–1.1 eV) associated with doubly ionized oxygen vacancies ( $V_o^{\cdot\cdot}$ ) common in perovskite oxide ferroelectrics. Electrical imbalance produced by acceptor dopant, such as  $\text{Mg}^{2+}$ , is compensated by these anionic defects [11]. Dielectric characterization was conducted on  $\text{PbTi}_{0.5}\text{Zr}_{0.3}(\text{Co}_{1-x}\text{Mg}_x)_{0.2}\text{O}_3$  ceramic system to understand the dielectric response of final materials.

## 2 Experimental

### 2.1 Sample preparation

Polycrystalline  $\text{PbTi}_{0.5}\text{Zr}_{0.3}(\text{Co}_{1-x}\text{Mg}_x)_{0.2}\text{O}_3$  ( $x = 0.00, 0.25, 0.45, 0.65, 0.85$ ) powders and ceramics were prepared by sol–gel route. Reagent grade lead acetate ( $\geq 99.5\%$ ), cobalt acetate tetra-hydrate (99.5%), magnesium acetate tetra-hydrate (98%), zirconium n-butoxide 80% in n-butanol, titanium isopropoxide (95%), acetyl-acetone (99.5%) and isopropanol were used as the starting materials. Stoichiometric amount of titanium isopropoxide was dissolved in isopropanol at room temperature. Acetylacetone was added to the solution to make a stable Ti-solution. Zirconium n-butoxide was added to the stable Ti-solution. Lead acetate tetra-hydrate, cobalt acetate tetra-hydrate and magnesium acetate tetra-hydrate were dissolved in a mixture of acetic acid and water at 80 °C for 2 h. Mixed metal ion (Pb, Co, Mg) solution was slowly added to Ti/Zr-solution. In a subsequent step 5 ml of water was added to above mixture to form a clear sol. The solution was stirred for 2 h at 80 °C until a stable sol was obtained. The sol was dried at 120 °C overnight in order to make xerogel. The

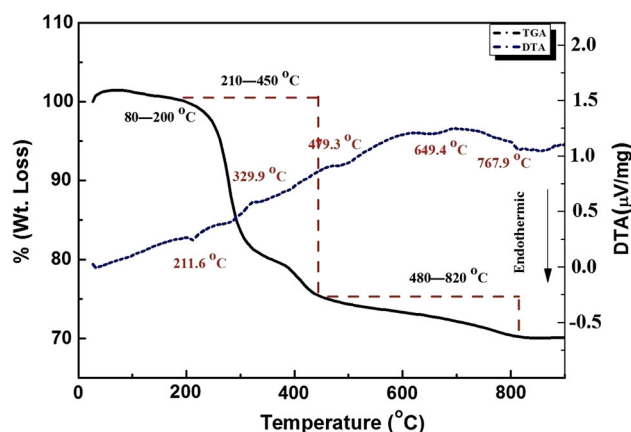
xerogel was calcined at 750 °C for 2 h to obtain  $\text{PbTi}_{0.5}\text{Zr}_{0.3}(\text{Co}_{1-x}\text{Mg}_x)_{0.2}\text{O}_3$  powders. Polyvinyl butyral (PVB) binder was added in 5 wt% to the resultant powders and mix-milled in agate and mortar for 15 min. The powders were then pressed into pellets and binder was burned out at 600 °C for 30 min with a heating step size of 5 °C/min and subsequently sintered at 1150 °C for 2 h to get dense ceramics. The ceramic samples were used for further characterization.

### 2.2 Characterization

X-ray diffraction (XRD) measurements were carried out at room temperature in order to investigate phase purity with a DMAX 2200 (Rigaku Corp, Japan) X-ray diffractometer using Ni-filtered  $\text{Cu-K}\alpha$  radiation ( $\lambda = 1.5418$  Å) for  $2\theta = 20^\circ\text{--}70^\circ$  with step size of  $0.02^\circ$ . Scanning electron microscopy (SEM) was used in order to investigate the microstructure of sintered ceramics using a XL30 (FEI Co., USA) scanning electron microscope operating at 15 keV. The electrical measurements were performed on parallel-plate capacitor configuration using an Agilent, HP 4194A LCR-meter. Polished surfaces of the sintered pellets were coated with Ag-paste and fired at 600 °C for 30 min in order to make the electrodes. Impedance of the samples was monitored between 30 and 300 °C, with accuracy better than 0.1 °C by using NOVOTHERM Temperature Control System.

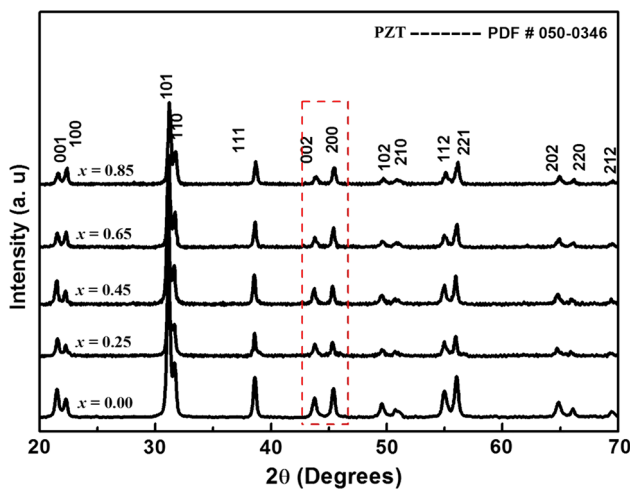
## 3 Results and discussion

Figure 1 shows TG/DTA curves recorded in air for the  $\text{PbTi}_{0.5}\text{Zr}_{0.3}(\text{Co}_{1-x}\text{Mg}_x)_{0.2}\text{O}_3$  precursor gel. A continuous decrease in the dried gel TG trace due to weight loss was



**Fig. 1** TG/DTA for the  $\text{PbTi}_{0.5}\text{Zr}_{0.3}(\text{Co}_{1-x}\text{Mg}_x)_{0.2}\text{O}_3$  xerogel synthesized by sol–gel method

observed up to 820 °C. This curve can be divided into three major regions; 80–200 °C, 210–450 °C and 480–820 °C. The first step weight loss in the temperature regime from 80 to 200 °C was associated with the removal of residual water and low boiling point organic solvents. A fraction of organic matter also decomposes in this temperature range. This step was accompanied by another small endothermic dip on the DTA curve around 130 °C [12]. The second step weight loss (210–450 °C) was attributed to the more complex reactions which involved both exothermic and endothermic reactions. This step involves the pyrolysis of acetates, removal of high boiling point organic compounds and rearrangement of chemical bonds, where gel is converted into a polymer. This step was accompanied by endothermic (211.6 °C) peak and exothermic (329.9; 479.3 °C) peaks on DTA curve [13]. The third step involved continuous weight loss in the temperature regime from 480 to 820 °C. This step corresponds to the decarburization and the formation of the new phase. Various polymeric networks in the gel are decomposed and metal oxides formed subsequently reacts in this temperature regime to form the final product [14, 15]. This step is accompanied by broad endothermic (650; 770 °C) and exothermic (600; 700; 810 °C) peaks on DTA curve.



**Fig. 2** XRD patterns for the  $\text{PbTi}_{0.5}\text{Zr}_{0.3}(\text{Co}_{1-x}\text{Mg}_x)_{0.2}\text{O}_3$  ceramic samples

Beyond 820 °C no changes could be traced in the TG curve which confirmed the formation of the final product.

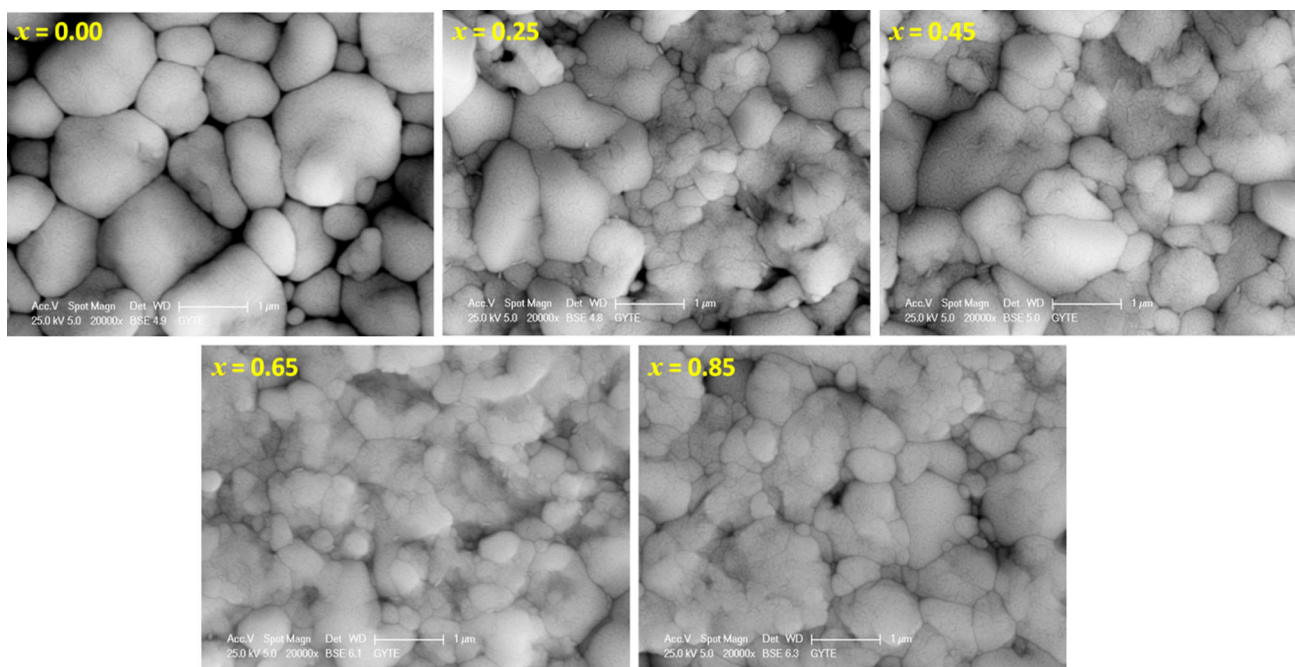
Figure 2 presents XRD pattern for the  $\text{PbTi}_{0.5}\text{Zr}_{0.3}(\text{Co}_{(0.2)1-x}\text{Mg}_x)_{0.2}\text{O}_3$  ( $x = 0.00, 0.25, 0.45, 0.65, 0.85$ ) ceramic samples. Observed increase in the intensity as well as sharpness of the XRD peaks for sintered samples indicated well crystallized  $\text{PbTi}_{0.5}\text{Zr}_{0.3}(\text{Co}_{(0.2)1-x}\text{Mg}_x)_{0.2}\text{O}_3$  material and no secondary phases were observed in all samples, which confirmed the incorporation of Co and Mg in the PZT crystal structure. The XRD peaks could be indexed according to the tetragonal symmetry ( $P4mm$ , PDF # = 00-050-0346) as splitting around  $2\theta \sim 45^\circ$  was observed in all ceramic samples [16]. The crystallite sizes calculated from the XRD data are given in the Table 1. The intensity of Mg doped samples is low compared to undoped sample. These variations in relative peak intensity and the corresponding shifts in the peak positions are associated with the presence of strains (uniform and non-uniform) in the crystal lattice due to the increase content of different ionic radii (i.e.,  $\text{Mg}^{2+}$ ,  $\text{Co}^{3+}$ ) compared to  $\text{Ti}^{4+}$ .

Figure 3 shows the SEM micrographs for the polished surface of  $\text{PbTi}_{0.5}\text{Zr}_{0.3}(\text{Co}_{1-x}\text{Mg}_x)_{0.2}\text{O}_3$  ceramics at high resolution. SEM micrographs of the surface showed well connected grain microstructure with limited porosity, which is often associated with PbO based ceramics. A considerable decrease in the average grain size was observed in the compositions doped with high Mg content, which acted as grain growth inhibitor. Increasing concentration of Mg resulted in at more homogeneous particle morphology and the density of ceramics was increased with an increase in Mg content.

Figure 4a shows temperature dependent dielectric response of  $\text{PbTi}_{0.5}\text{Zr}_{0.3}(\text{Co}_{1-x}\text{Mg}_x)_{0.2}\text{O}_3$  ceramics measured at 100 kHz. Magnitude of  $\epsilon_r$  increased gradually with increasing temperature. Phase transition temperature was not observed in the current experimental setup. The  $T_c$  for the doped-PZT ceramics can be predicted beyond 300 °C, which can be observed from the current dielectric curve trend with temperature. Due to the dominant behavior of the interfacial polarization compared to dipolar polarization the magnitude of  $\epsilon_r$  increases with temperature [17, 18]. Magnitude of  $\epsilon_r$  (4261) for the sample with  $x = 0.25$  was high at room temperature which decreased gradually

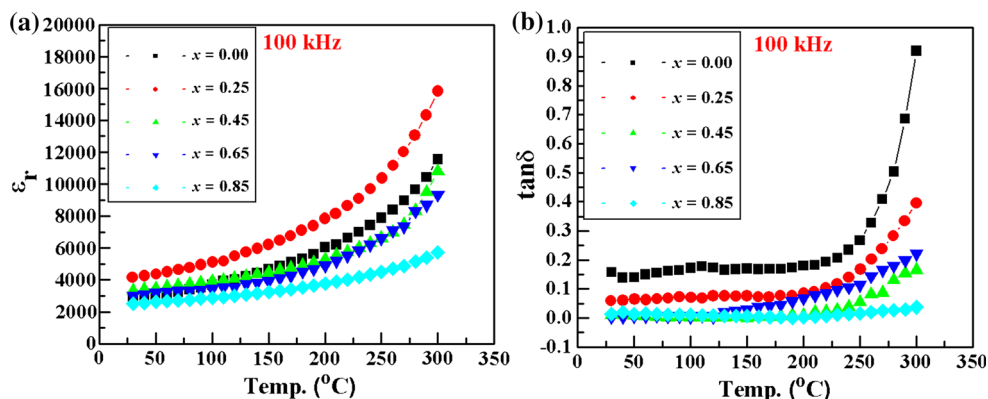
**Table 1** Crystallite size calculated from FWHM and room temperature dielectric properties of  $\text{PbTi}_{0.5}\text{Zr}_{0.3}(\text{Co}_{(0.2)1-x}\text{Mg}_x)_{0.2}\text{O}_3$  at 100 kHz

Sample	FWHM	Crystallite size (nm)	Room T° $\epsilon_r$ (100 kHz)	Room T° $\tan\delta$ (100 kHz)
$x = 0.00$	0.42752	20	2804	0.15
$x = 0.25$	0.4315	20	4261	0.05
$x = 0.45$	0.3197	26	3342	0.004
$x = 0.65$	0.3137	27	3011	0.009
$x = 0.85$	0.3920	21	2515	0.01



**Fig. 3** SEM micrographs of the thermally etched surface of  $\text{PbTi}_{0.5}\text{Zr}_{0.3}(\text{Co}_{1-x}\text{Mg}_x)_{0.2}\text{O}_3$  ceramics

**Fig. 4** Dielectric properties of the  $\text{PbTi}_{0.5}\text{Zr}_{0.3}(\text{Co}_{1-x}\text{Mg}_x)_{0.2}\text{O}_3$  ceramics with temperature



with an increase in Mg content up to 2444 for the sample with  $x = 0.85$  at 100 kHz.

Figure 4b shows variation of  $\tan\delta$  with temperature measured at 100 kHz. The  $\tan\delta$  was constant to a wide range of temperature and then tempted to increase with further increase in temperature. This increase in  $\tan\delta$  is associated with various factors; such as % porosity, inherent defects in the material and defects developed during processing [19, 20]. The magnitude of  $\tan\delta$  was decreased with an increase in Mg content. It has been reported that the magnitude of  $\tan\delta$  for the  $\text{MgTiO}_3$  is very low, so an increase in Mg content was responsible for a decrease in the net  $\tan\delta$  in the  $\text{PbTi}_{0.5}\text{Zr}_{0.3}(\text{Co}_{1-x}\text{Mg}_x)_{0.2}\text{O}_3$  ceramics. The magnitude of  $\tan\delta$  for the sample with  $x = 0.00$  was measured as  $\tan\delta = 0.1$  around room

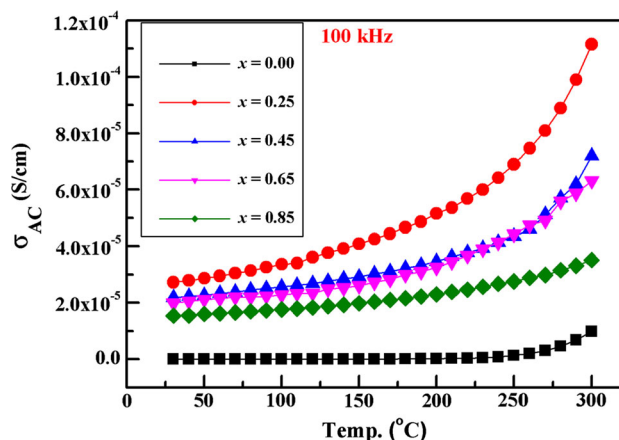


**Fig. 5** AC conductivity of the  $\text{PbTi}_{0.5}\text{Zr}_{0.3}(\text{Co}_{1-x}\text{Mg}_x)_{0.2}\text{O}_3$  ceramics with temperature

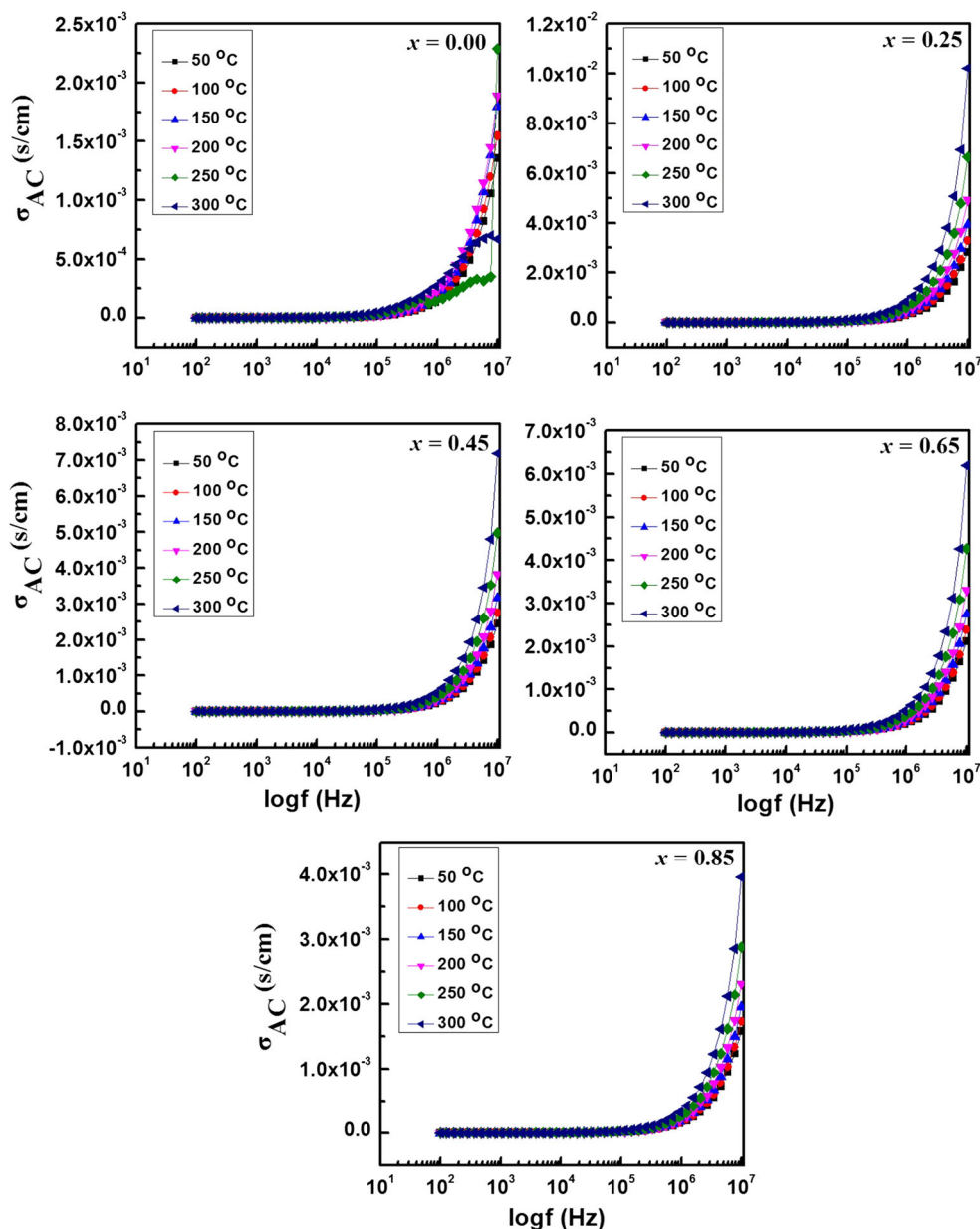
temperature, which was decreased to 0.01 for the  $x = 0.65$  composition around room temperature.

The conduction mechanism of the  $\text{PbTi}_{0.5}\text{Zr}_{0.3}(\text{Co}_{1-x}\text{Mg}_x)_{0.2}\text{O}_3$  ceramic samples were evaluated by measuring the AC conductivity at 100 kHz in the temperature regime from room temperature to 300 °C. The results are presented in the Fig. 5. AC conductivity of the  $x = 0.00$  composition was independent of the temperature in the low temperature regime up to 250 °C which then gradually increased with further increase in temperature. Mg doping resulted in an increase in the conductivity which was gradually decreased for the high doped Mg content. Sample

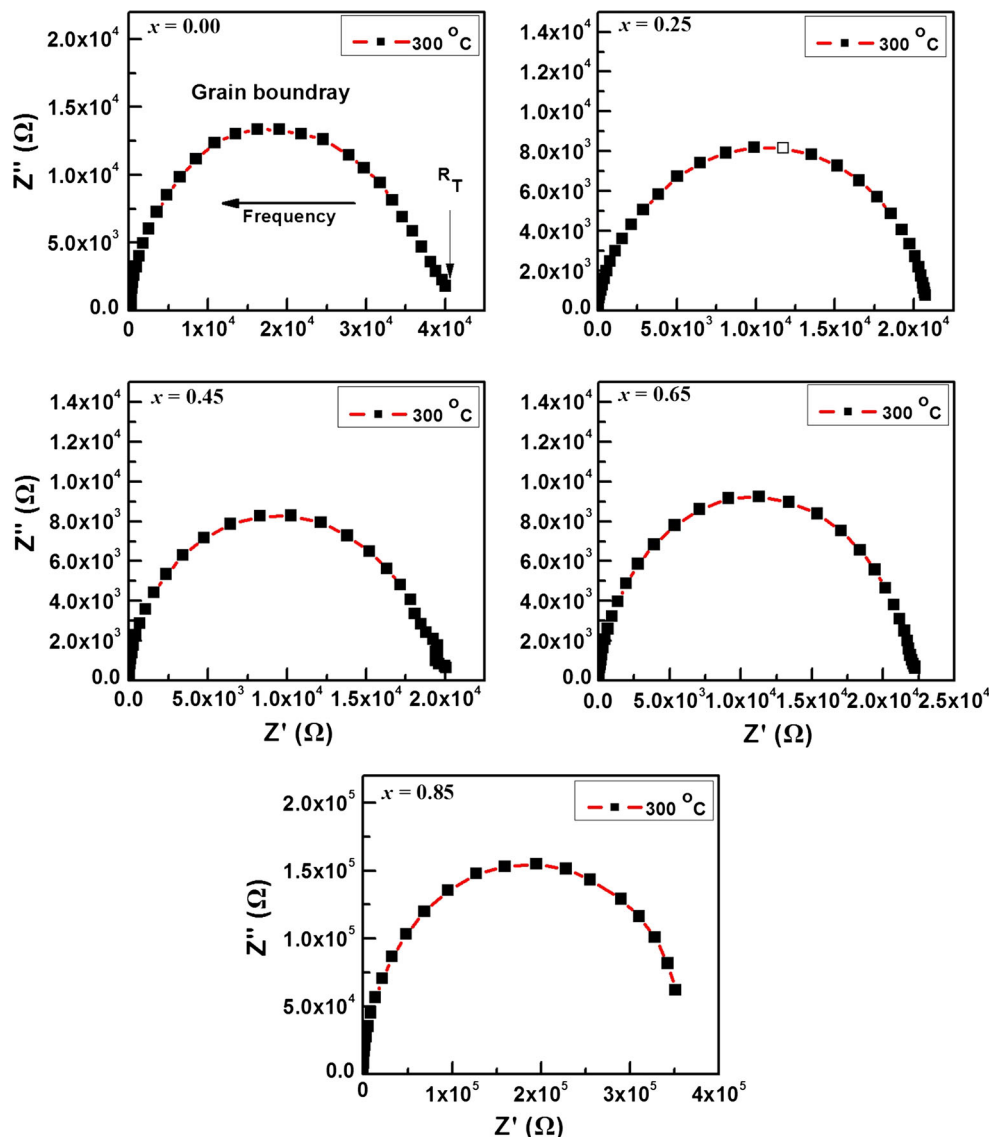
with  $x = 0.25$  exhibited high magnitude of conductivity in the given temperature regime.

Figure 6 shows variation of AC conductivity of the  $\text{PbTi}_{0.5}\text{Zr}_{0.3}(\text{Co}_{1-x}\text{Mg}_x)_{0.2}\text{O}_3$  ceramic samples with frequency at various temperatures. There is no remarkable difference in the conductivity of the  $x = 0.00$ – $0.85$  compositions in the low frequency regime (up to  $\approx 10^5$  Hz), which increased abruptly with further increase in frequency for all the ceramic samples. Moreover, this behavior was observed at low frequency with an increase in temperature. The variation of conductivity with frequency can be associated with the fact that at low frequency the charged

**Fig. 6** AC conductivity of the  $\text{PbTi}_{0.5}\text{Zr}_{0.3}(\text{Co}_{1-x}\text{Mg}_x)_{0.2}\text{O}_3$  ceramics with frequency at various temperatures



**Fig. 7** Cole-Cole plots for the  $\text{PbTi}_{0.5}\text{Zr}_{0.3}(\text{Co}_{1-x}\text{Mg}_x)_{0.2}\text{O}_3$  ceramics at 300 °C



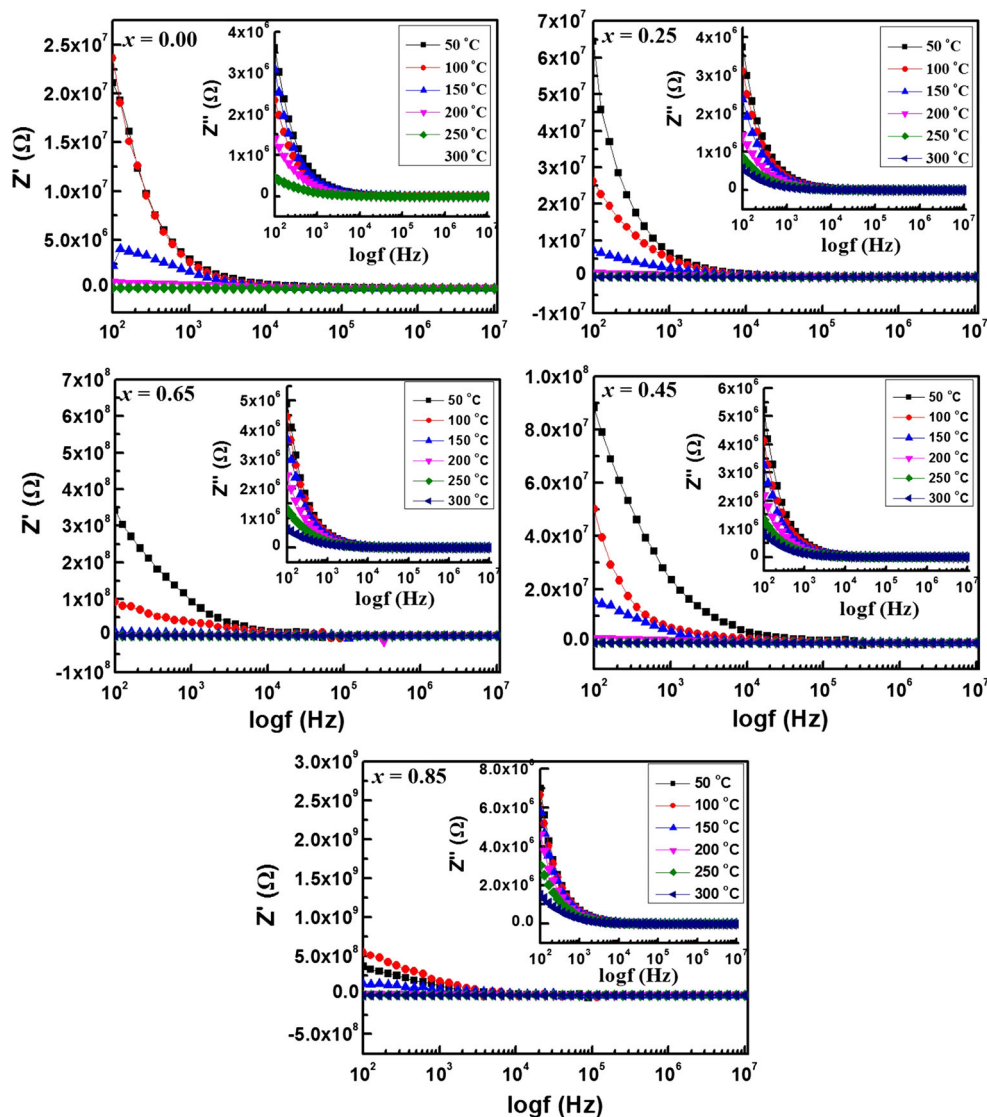
species are mobile for long distances as opposed to the charge relaxation which becomes operative at high frequencies. The low magnitude of conductivity at wide range of frequency can be associated with the production of oxygen vacancies by acceptor doped  $\text{Co}^{3+}$  and  $\text{Mg}^{2+}$  for  $\text{Ti}^{4+}/\text{Zr}^{4+}$  site in PZT perovskite crystal structure. Oxygen vacancies created in the PZT structure by these dopants acts as electron trap sites, which can be activated thermally and results in an increase in the AC conductivity [21].

Figure 7 shows Cole–Cole (Nyquist plots), obtained by plotting  $Z'$  versus  $Z''$  at various temperatures for the  $\text{PbTi}_{0.5}\text{Zr}_{0.3}(\text{Co}_{1-x}\text{Mg}_x)_{0.2}\text{O}_3$  ceramic samples. The plot showed single semicircular arcs (at 300 °C) throughout the investigated frequency range (100 Hz–1 MHz) for all the ceramic samples. A complete semicircle was not obtained for the  $x = 0.85$  composition at 300 °C. The semicircles

are depressed to certain degrees which showed deviation from ideal behavior. Such behavior can be associated with the overlapping of two or more semicircles which could not be resolved in the current experimental setup. The semicircle at low frequency is associated with the grain boundary contributions and at high frequency corresponds to the bulk (grain) contribution [22]. Total resistance ( $R_T$ ) was calculated from a polynomial fit to the semicircles and the magnitude was obtained from the intercept along x-axis. Magnitude of the resistance was observed to decrease with an increase in temperature.

Figure 8 shows variation of  $Z'$  with frequency at selected temperatures. Magnitude of  $Z'$  decreased monotonically with increasing frequency and became independent of frequency after certain values and merges to some low values. This trend of attaining the consistent values

**Fig. 8**  $Z'$  and  $Z''$  with frequency for the  $\text{PbTi}_{0.5}\text{Zr}_{0.3}(\text{Co}_{1-x}\text{Mg}_x)_{0.2}\text{O}_3$  ceramics

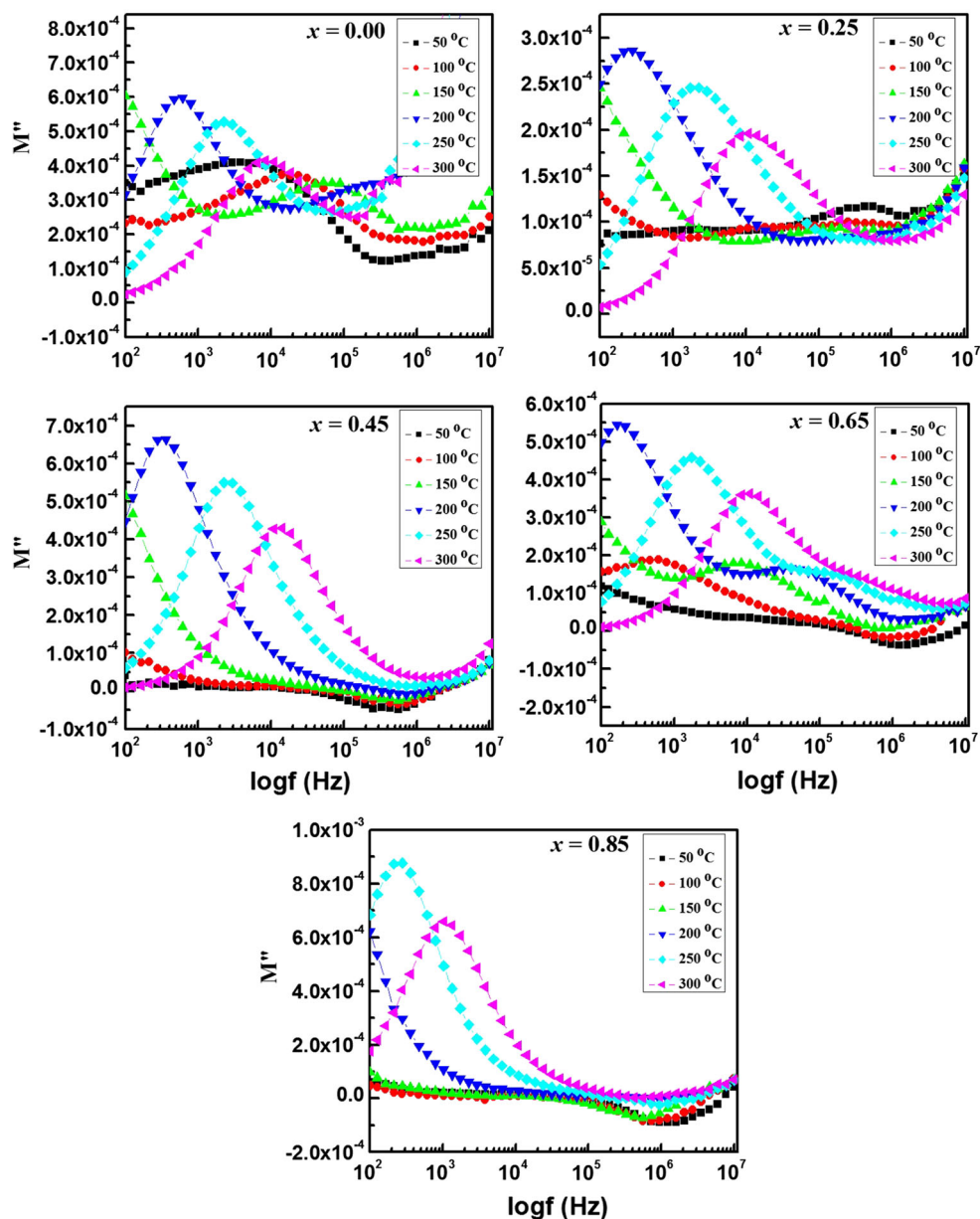


also shifted gradually toward low frequency regime with an increase in temperature. This effect might be due to the increasing of barrier properties associated with the possible trapping of space charge [23]. The inset figures present the variation of  $Z''$  with frequency at selected temperatures. Magnitude of  $Z''$  was decreased with increasing frequency and temperature and became independent of both temperature and frequency in the high frequency regime. The magnitude of  $Z''$  was decreased with an increase in temperature.

Figure 9 shows variation of  $M''$  versus frequency for the  $\text{PbTi}_{0.5}\text{Zr}_{0.3}(\text{Co}_{1-x}\text{Mg}_x)_{0.2}\text{O}_3$  ceramics at various temperatures. Only one peak was observed for  $M''$  at high frequency which might be due to the bulk contribution. Both

$Z''$  and  $M''$  highlight different features of the materials. Since height of the  $Z''$  peak ( $Z''_{\text{max}}$ ) is equal to  $R/2$  for that particular element, the  $Z''$  plot is associated with the most resistive elements of the material.  $M''$  plots are associated to the smallest capacitance since  $M''$  peak maximum is given by  $\epsilon_0/2C$  ( $\epsilon_0$  is the permittivity of free space,  $8.854 \times 10^{-14} \text{ Fcm}^{-1}$ ) for that particular element. Materials which are electrically inhomogeneous (i.e. have different bulk, grain boundary and electrode characteristics) require more than one RC elements for their description, and as a result the  $Z''$  and  $M''$  plot looks different [24]. Such variation in the  $Z''$  and  $M''$  plots confirmed both grain boundary and bulk contribution in the  $\text{PbTi}_{0.5}\text{Zr}_{0.3}(\text{Co}_{1-x}\text{Mg}_x)_{0.2}\text{O}_3$  ceramics.

**Fig. 9**  $M''$  with frequency for the  $\text{PbTi}_{0.5}\text{Zr}_{0.3}(\text{Co}_{1-x}\text{Mg}_x)_{0.2}\text{O}_3$  ceramics



#### 4 Conclusion

Polycrystalline  $\text{PbTi}_{0.5}\text{Zr}_{0.3}(\text{Co}_{1-x}\text{Mg}_x)_{0.2}\text{O}_3$  ceramics were successfully synthesized at 1150 °C for 2 h in air by using sol–gel route. Microstructure of ceramic samples was found to be dependent on Mg doping content. Magnitude of  $\tan\delta$  and  $\epsilon_r$  of  $\text{PbTi}_{0.5}\text{Zr}_{0.3}(\text{Co}_{1-x}\text{Mg}_x)_{0.2}\text{O}_3$  ceramic samples was decreased with an increase in Mg content. Sample with  $x = 0.25$  was found to exhibit a high  $\epsilon_r$  (4261) and  $\tan\delta$  (0.05) around room temperature at 100 kHz. Complex impedance spectroscopic analysis revealed that  $\text{PbTi}_{0.5}\text{Zr}_{0.3}(\text{Co}_{1-x}\text{Mg}_x)_{0.2}\text{O}_3$  ( $x = 0.00$ – $0.85$ ) exhibited both grain boundary and bulk contributions, which could not be confirmed from Cole–Cole plots. Total resistance was

decreased with increasing temperature showing a typical ceramic behavior. AC conductivity was increased with increasing temperature due to the production of oxygen vacancies associated with doping of aliovalent dopants ( $\text{Co}^{3+}$ ,  $\text{Mg}^{2+}$ ) on B-site ( $\text{Ti}^{4+}/\text{Zr}^{4+}$  sites).

**Acknowledgments** The authors acknowledge the financial support by the Scientific and Technological Research Council of Turkey (TUBITAK) under the 2216-Fellowship Program for International Students.

#### References

- C.P. Shaw, S. Gupta, S.B. Stringfellow, A. Navarro, J.R. Alcock, R.W. Whatmore, *J. Eur. Ceram. Soc.* **22**, 2123 (2002)



2. X.P. Jiang, W.P. Chen, Z. Peng, M. Zeng, H.L.W. Chan, C.L. Choy, Q.R. Yin, *Ceram. Int.* **32**, 583 (2006)
3. M.D. Nguyena, T.Q. Trinha, M. Dekkers, E.P. Houwman, H.N. Vua, G. Rijnders, *Ceram. Int.* **40**, 1013 (2014)
4. Q. Zhang, T. Yang, Y. Zhang, X. Yao, *J. Alloys Compd.* **583**, 254 (2014)
5. R. Rai, S. Mishrab, N.K. Singh, *J. Alloys Compd.* **487**, 494 (2009)
6. V.A. Chaudhari, G.K. Bichile, *Phys. B* **405**, 534 (2010)
7. S. Jiang, L. Zhang, G. Zhang, S. Liu, J. Yi, X. Xiong, Y. Yu, J. He, Y. Zeng, *Ceram. Int.* **39**, 5571 (2013)
8. Q. Meng, K. Zhu, X. Pang, J. Qiu, B. Shao, H. Ji, *Adv. Powder Technol.* **24**, 212 (2013)
9. H.-L. Huang, G.Z. Cao, I.Y. Shen, *Sens. Actuators, A* **214**, 111 (2014)
10. C.A. Oliveiran, E. Longo, J.A. Varela, M.A. Zaghete, *Ceram. Int.* **40**, 1717 (2014)
11. B. Guiffard, E. Boucher, L. Eyraud, L. Lebrun, D. Guyomar, *J. Eur. Ceram. Soc.* **25**, 2487 (2005)
12. H. Singh, A. Kumar, K.L. Yadav, *Mater. Sci. Eng. B* **176**, 540 (2011)
13. L. Li, J. Song, Q. Lu, X. Tann, *Ceram. Int.* **40**, 1189 (2014)
14. H. Jena, K.V.G. Kutty, T.R.N. Kutty, *Mater. Chem. Phys.* **88**, 167 (2004)
15. R.B. Cervera, Y. Oyama, S. Yamaguchi, *Solid State Ion* **178**, 569 (2007)
16. R. Tipakontitukul, S. Ananta, *Mater. Lett.* **58**, 449 (2004)
17. J.Y. Wu, J.J. Bian, *Ceram. Int.* **38**, 3217 (2012)
18. S.-F. Wang, Y.-R. Wang, C.-Y. Liu, W.-S. Hsieh, *Ceram. Int.* **38**, 1127 (2012)
19. E.S. Kim, H.S. Park, K.H. Yoon, *Mater. Chem. Phys.* **79**, 213 (2003)
20. S. Basu, K.R. Babu, R.N.P. Choudhary, *Mater. Chem. Phys.* **132**, 570 (2012)
21. B. Behera, P. Nayak, R.N.P. Choudhary, *Mater. Chem. Phys.* **106**, 193 (2007)
22. A. Mishra, S.N. Choudhary, K. Prasad, R.N.P. Choudhary, *Phys. B* **406**, 3279 (2011)
23. H. Singh, A. Kumar, K.L. Yadav, *Mater. Sci. Eng. B* **176**, 540 (2011)
24. J.T.S. Irvine, D.C. Sinclair, A.R. West, *Adv. Mater.* **2**, 132 (1990)